Shape Sensitivities of Capacitances of Planar Conducting Surfaces Using the Method of Moments

Jan Ureel, *Student Member, IEEE*, and Daniël De Zutter, *Member, IEEE*

Abstract—**In this contribution, a new method is presented to obtain the sensitivities of the capacitance or the charge with respect to a geometrical parameter of planar conducting surfaces. The charge density is found by an integral equation technique. By applying the flux-transport theorem, a new integral equation for the total derivative of the charge with respect to a geometrical parameter is derived from the original electrostatic integral equation for the charge distribution. This new integral equation is solved together with the original integral equation by the method of moments using the same set of basis and test functions. The method is also applied to obtain derivatives for the inductance, impedance and effective dielectric constant. Some simple electrostatic problems are presented, which illustrate the capabilities of our approach. In these examples we also discuss the difference between the geometrical derivatives obtained in this way with geometrical derivatives which are obtained by a central finite difference estimate. Next, some examples of the calculation of geometrical derivatives of capacitance and inductance matrices of multilayer, multiconductor thin microstrip lines are discussed.**

I. Introduction

THE ANALYSIS of electromagnetic problems by various numerical methods such as the finite element method (FEM), method of moments (MoM), finite-difference time-domain (FDTD) technique, or transmission line method (TLM) has undergone an exponential growth in the last two decades through the availability of powerful computing resources. In the case of magnetostatics, electrodynamics, or microwave circuits, e.g., the use of electromagnetic simulators is already well established [1]. For microstrip filter design, attention recently focused on the application of electromagnetic simulators in the design process [2] which leads to the realization of automated nominal design, sensitivity analysis, and yield analysis based on a rigorous electromagnetic analysis.

Efficient optimization methods make use of derivative information of the cost or performance function with respect to some geometrical parameter of the considered structure. These first derivatives are not readily available in electromagnetic simulators. Clever error function fitting or interpolation schemes are therefore invented to approximate these derivatives [3], [4]. For the FEM-analysis, a successful attempt has been made to directly obtain the derivatives during electromagnetic simulation [5]. For the MoM or the FDTD, no publications in that direction are known to the authors.

Our efforts aim at the direct calculation of geometrical derivatives when the analysis is based on a MoM technique. Because this research topic is quite new and in order to illustrate the basic principles, we restrict ourselves in this paper to the MoM used as an analysis method for electrostatic problems of the following type: planar perfectly conducting surfaces of a general shape embedded in a planar stratified medium in two or three dimensions. A method is proposed to calculate the derivative of the unknown charge density with respect to some geometrical parameter of the surface. Therefore, a new integral equation (IE) is derived from the original electrostatic integral equation starting from a transport theorem. Next, a general, computationally efficient procedure using the MoM for solving this IE is presented. We also investigate the relationship between meshing strategies and the process for obtaining the desired derivative. The applicability of the new IE is illustrated by some simple electrostatic examples found in [6]–[8].

The work presented here sets forth some general principles that will be extended to the full-wave analysis of microstrip lines and MMIC's. This will be presented in a forthcoming paper.

The outline of this paper is as follows: in Section II we derive a new IE for the total derivative of the charge density with respect to some geometrical parameter of the conducting surface. In Section III the possible singularities of the kernel in this new IE are discussed. It will be formally proved that these singularities are of the same order as in the original IE for the charge density. In Section IV the IE is validated by the analytically known example of the charge distribution on a disk. A general computationally efficient method for solving both the new IE and the original IE by the MoM is outlined in Section V. In Sections VI and VII we illustrate this general method with some simple electrostatic examples. For the case of a single conducting patch in free space, we discuss the difference between the geometrical derivatives, obtained from the new IE and an estimation of the derivatives based on a central difference formula and on repeated evaluation of the charge density for geometrically different surfaces. It will be shown that the way in which the meshing is performed will greatly influence this finite difference estimate. In Section VII we demonstrate that the method can be applied to obtain derivatives with respect to the distance between surfaces. The subsequent examples in Section VIII demonstrate the applicability of the new method for the calculation of the derivatives of the characteric impedance and effective dielectric constant of a multilayer thin microstrip line and the derivative of the mode-impedances of multiconductor lines.

Manuscript received July 22, 1994, revised November 12, 1995.

The authors are with the Department of Information Technology, Universiteit Gent, Sint-Pietersnieuwstraat 41, B-9000 Gent, Belgium.

Publisher Item Identifier S 0018-9480(96)01443-3.

II. Integral Equation for the Geometrical Derivative of the Charge

In electrostatics, the potential and charge distribution on a perfectly conducting surface of general shape are related to each other by the IE

$$V(\bar{r}) = \iint_{S_\xi} G(\bar{r}\,|\,\bar{r}')q(\bar{r}')dS' \tag{1}$$

where $V(\bar{r})$ is the potential on the surface (or union of surfaces) S_ξ, $q(\bar{r}')$ is the unknown charge distribution on the surface and $G(\bar{r}\,|\,\bar{r}')$ is a suitable Green's function kernel [9]. We assume that the metallisations are embedded in a planar stratified medium (homogeneous and isotropic) which extends infinitely in the x- and y-directions. Furthermore we suppose that ξ represents a geometrical parameter which in some way modifies the position of the surface in the plane or the shape of the surface itself. The considered surfaces can be translated, expanded, or shrunk, when ξ is varied.

We review the flux transport theorems of Helmholtz and Reynolds [10]. If the flux of a vector field $\bar{F}$ through a surface S_ξ, which depends on a geometrical parameter ξ is given by

$$\Phi = \iint_{S_\xi} \bar{F} \cdot d\bar{S} \tag{2}$$

then the total derivative of this flux is given by

$$\frac{d\Phi}{d\xi} = \iint_{S_\xi} \left[\frac{\partial \bar{F}}{\partial \xi} + \bar{v}\bar{\nabla}\cdot\bar{F}\right]\cdot d\bar{S} + \int_{\partial S_\xi} (\bar{F}\times\bar{v})\cdot d\bar{r} \tag{3}$$

where ∂S_ξ is the circumference of the surface S_ξ and $\bar{v} = d\bar{r}/d\xi$ is the velocity of a point located on the surface. An equivalent expression for (3) is

$$\frac{d\Phi}{d\xi} = \iint_{S_\xi} \left[\frac{\partial \bar{F}}{\partial \xi} + (\bar{v}\cdot\bar{\nabla})\bar{F} + \bar{F}(\bar{\nabla}\cdot\bar{v}) - (\bar{F}\cdot\bar{\nabla})\bar{v}\right]\cdot d\bar{S}. \tag{4}$$

We prefer (4) over (3) since it is purely a surface integration without a boundary contribution. If the surface S_ξ moves or expands in a plane in space with normal unit vector $\bar{u}_z$ and if the vector field is of the form $\bar{F} = U\bar{u}_z$, we can rewrite expressions (3) and (4) as

$$\frac{d\Phi}{d\xi} = \iint_{S_\xi} \frac{\partial U}{\partial \xi} dS + \int_{\partial S_\xi} (U\bar{u}_z\times\bar{v})\cdot d\bar{r} \tag{5}$$

$$\frac{d\Phi}{d\xi} = \iint_{S_\xi} \left[\frac{\partial U}{\partial \xi} + (\bar{v}\cdot\bar{\nabla})U + U(\bar{\nabla}\cdot\bar{v})\right] dS \tag{6}$$

where the velocity, in this case reduces to

$$\bar{v} = \frac{dx}{d\xi}\bar{u}_x + \frac{dy}{d\xi}\bar{u}_y \tag{7}$$

with $\bar{u}_x$ and $\bar{u}_y$ the unit vectors in x- and y-direction. This is also known as the Reynolds theorem which is formulated here in two dimensions [10].

We will now apply the Reynolds theorem to the IE (1). The theorem as given by (6) is the easiest to deal with because the charge distribution becomes singular at the boundary of the surface [11] and thus the line integral in (5) is to be defined as a limiting value, which complicates calculations. Therefore, we restrict our attention to the form (6) of the theorem. The excitation position vector $\bar{r}'$ is a function of the geometrical parameter ξ if the surface is modified by this geometrical parameter. Likewise, the observation position vector $\bar{r}$ can be a function of ξ, if the observation point is located on the surface S_ξ. Taking the derivative of the right- hand side of IE (1) with respect to ξ for all quantities that depends on $\bar{r}'$ and ignoring the dependence of $\bar{r}$ on ξ leads to the term

$$\iint_{S_\xi} \left[G(\bar{r}\,|\,\bar{r}')\left(\frac{\partial}{\partial\xi}q(\bar{r}') + \bar{v}'\cdot\bar{\nabla}'q(\bar{r}')\right) + \bar{\nabla}'.\bar{v}'G(\bar{r}\,|\,\bar{r}')q(\bar{r}') + \bar{v}'\cdot\bar{\nabla}'G(\bar{r}\,|\,\bar{r}')q(\bar{r}')\right]dS' \tag{8}$$

where $\bar{v}' = \bar{v}(\bar{r}')$. To obtain this result, we applied the flux-transport theorem and expressed the fact that the Green's function is independent of the geometrical parameter ξ itself for each point in space, i.e., $\partial G(\bar{r}\,|\,\bar{r}')/\partial\xi = 0$. The complete derivative of the IE (1) with respect to ξ, taking into account the dependence of $\bar{r}$ upon ξ, follows

$$\begin{aligned}\frac{\partial}{\partial\xi}V(\bar{r}) + \bar{v}\cdot\bar{\nabla}V(\bar{r}) &= \iint_{S_\xi}\left[G(\bar{r}\,|\,\bar{r}')\left(\frac{\partial}{\partial\xi}q(\bar{r}') + \bar{v}'\cdot\bar{\nabla}'q(\bar{r}')\right)\right.\\ &\quad + (\bar{\nabla}'\cdot\bar{v}')G(\bar{r}\,|\,\bar{r}')q(\bar{r}') + \bar{v}'\cdot\bar{\nabla}'G(\bar{r}\,|\,\bar{r}')q(\bar{r}')\\ &\quad \left. + \bar{v}\cdot\bar{\nabla}G(\bar{r}\,|\,\bar{r}')q(\bar{r}')\right]dS'.\end{aligned} \tag{9}$$

The first three terms in the integrand of (9) stem directly from (8). By introducing the new unknown variable $p(\bar{r}') = \frac{\partial}{\partial\xi}q(\bar{r}') + \bar{v}'\cdot\bar{\nabla}'q(\bar{r}')$, which is the total derivative of the charge density at a point with respect to the parameter ξ, and noting the fact that the Green's function only depends upon $|\bar{r} - \bar{r}'|$, a new IE can be formulated as follows

$$\begin{aligned}\frac{\partial}{\partial\xi}V(\bar{r}) + \bar{v}\cdot\bar{\nabla}V(\bar{r}) &= \iint_{S_\xi}[G(\bar{r}\,|\,\bar{r}')p(\bar{r}') + (\bar{\nabla}'\cdot\bar{v}')G(\bar{r}\,|\,\bar{r}')q(\bar{r}')\\ &\quad + (\bar{v}' - \bar{v})\cdot\bar{\nabla}'G(\bar{r}\,|\,\bar{r}')q(\bar{r}')]dS'.\end{aligned} \tag{10}$$

Equivalently

$$\begin{aligned}\frac{\partial}{\partial\xi}V(\bar{r}) + \bar{v}\cdot\bar{\nabla}V(\bar{r}) &= \iint_{S_\xi} G(\bar{r}\,|\,\bar{r}')p(\bar{r}')dS'\\ &\quad + \iint_{S_\xi} \bar{\nabla}'\cdot[(\bar{v}' - \bar{v})G(\bar{r}\,|\,\bar{r}')]q(\bar{r}')dS'.\end{aligned} \tag{11}$$

If the total derivative of the potential and the charge density are known on the entire surface S_ξ, this IE can be solved for $p(\bar{r}')$. Since a perfectly conducting surface stands on a constant potential and the tangential electric field is zero on this surface, the left-hand side of (11) will be zero if $\bar{v}$ is tangential to the plane of S_ξ. First we notice that in (11) the same integral kernel $G(\bar{r}\,|\,\bar{r}')$ appears as in the original IE (1) and that a modified kernel of the form

$$\bar{\nabla}'\cdot[(\bar{v}' - \bar{v})G(\bar{r}\,|\,\bar{r}')] \tag{12}$$

appears in front of the charge density. Second, when a single surface S_ξ undergoes a translation, the velocity vector reduces to a constant vector ($\bar{v} = \bar{v}' = \bar{c}$) and the expected zero solution $p(\bar{r}')$ automatically follows from the new IE (11).

III. Singular Behavior of the Modified Kernel in the New Integral Equation

The Green's function kernel in three dimensions in the original IE (1) has a singularity of the form

$$[G(\bar{r} \mid \bar{r}')]_{\rho \to 0} \simeq C \frac{1}{|\bar{r} - \bar{r}'|} = \frac{C}{\rho} \tag{13}$$

with C some constant and $\rho = |\bar{r} - \bar{r}'|$. This is a weak singularity which can be integrated over a surface. In the modified kernel (12) a divergence term of the velocity together with a gradient term of the Green's function arises. The gradient of the singular part (13) of the Green's function with respect to the excitation vector is given by

$$[\bar{\nabla}' G(\bar{r} \mid \bar{r}')]_{\rho \to 0} \simeq C \frac{(\bar{r} - \bar{r}')}{|\bar{r} - \bar{r}'|^3}. \tag{14}$$

This is a strong singularity if the observation and excitation position vectors coincide. In that case, the second integral in (11) must be defined by its principal value. This mathematical difficulty disappears when the velocity vector has at least a component which is linear in x or y. If we assume that the velocity (7) is of the form $\bar{v}(\bar{r}) = (\alpha x + \beta y + \gamma)\bar{u}_x$, then the singular part of the third term of the right-hand side of (10) can be expanded as

$$\iint_{S_\xi} [\alpha(x' - x) + \beta(y' - y)] \frac{(x' - x)}{\rho^3} q(\bar{r}')\, dS'. \tag{15}$$

Using the transformation

$$\begin{cases} x' - x = \rho \cos\phi \\ y' - y = \rho \sin\phi \end{cases}. \tag{16}$$

The previous expression becomes

$$\iint_{S_\xi} \frac{\alpha \cos^2\phi + \beta \sin\phi \cos\phi}{\rho} q(\bar{r}') \rho d\rho d\phi \tag{17}$$

which shows that no strong singularities are in fact present. Therefore, we conclude that the singular behavior of the modified Green's kernel is not stronger than the one in the original IE, and hence the involved computational problems are not of a more severe nature.

IV. Charge Distribution on a Circular Disk

One of the few electrostatic three-dimensional examples where the charge density is known analytically is that of a circular disk on constant potential. The charge distribution for a circular disk having potential V_0 in a homogeneous, isotropic medium is given by the Maxwell distribution [11], [12]

$$q(r, a) = \frac{4V_0 \epsilon_0 \epsilon_r}{\pi} \frac{1}{\sqrt{a^2 - r^2}} \tag{18}$$

where a is the radius of the disk, r is the radial distance between a point on the disk and the origin, ϵ_0 the permittivity in vacuum, and ϵ_r the relative permittivity of the medium. The dependence of the charge on both r and a has been made explicit. We will validate the new IE (11) with this analytical example. The derivative of the charge density with respect to the geometrical parameter a is given by

$$\frac{\partial q(r, a)}{\partial a} = -M \frac{a}{\sqrt{(a^2 - r^2)^3}} \tag{19}$$

with $M = 4V_0 \epsilon_0 \epsilon_r / \pi$. The gradient vector is given by

$$\bar{\nabla} q(r, a) = \frac{\partial q(r, a)}{\partial r} \bar{u}_r = M \frac{r}{\sqrt{(a^2 - r^2)^3}} \bar{u}_r \tag{20}$$

where $\bar{u}_r$ is the unit vector in radial direction. Now consider an expansion of the disk in the radial direction with an amount Δa. The expansion is chosen such that each point on the disk moves over a distance given by $\Delta a(r/a)\bar{u}_r$, or has an expansion velocity of $\bar{v}(r, a) = (r/a)\bar{u}_r$. Hence $p(r, a)$ is given by

$$p(r, a) = -M \frac{1}{a\sqrt{a^2 - r^2}} = -\frac{q(r)}{a}. \tag{21}$$

In this case the total derivative of the charge density at each point is directly proportional to the charge density at that point. We check if the IE (11) above is fullfilled. The left-hand side of (11) is zero as $\bar{v}$ is a vector lying in the plane of the perfectly conducting disk. The second part of the right-hand side of the IE becomes, substituting the Green's function for a homogeneous medium

$$\begin{aligned} &\frac{1}{4\pi\epsilon_0\epsilon_r} \bar{\nabla}' \cdot \left[(\bar{v}' - \bar{v}) \frac{1}{\rho} \right] \\ &\quad = \frac{1}{4\pi\epsilon_0\epsilon_r} \left[\frac{1}{a} \bar{\nabla}' \cdot \frac{(x' - x)}{\rho} \bar{u}_x + \frac{(y' - y)}{\rho} \bar{u}_y \right] \\ &\quad = \frac{1}{4\pi\epsilon_0\epsilon_r} \frac{1}{a\rho}. \end{aligned} \tag{22}$$

The opposite result appears in the first part of the right-hand side of (11)

$$G(\bar{r} \mid \bar{r}') p(\bar{r}') = \frac{1}{4\pi\epsilon_0\epsilon_r} \left(-\frac{q(\bar{r}')}{a} \right) \frac{1}{\rho} \tag{23}$$

which leads to the desired zero result.

V. General Method for Solving the Integral Equation with the Method of Moments

We propose the following procedure for solving the pair of IE's (1) and (11): the IE (1) is solved in the "usual" manner with the MoM, i.e., we expand the unknown charge distribution over a set of N basis functions $B_j(\bar{r}')$ as

$$q(\bar{r}) \simeq q_N(\bar{r}) = \sum_{j=1}^{N} q_j B_j(\bar{r}') \tag{24}$$

and after testing with the N test functions $T_i(\bar{r})$ (1) results in a system of linear equations

$$V_i = \sum_{j=1}^{N} K_{ij} q_j \tag{25}$$

where K_{ij} and V_i are given by

$$K_{ij} = \iint_{S_\xi} T_i(\bar{r}) \iint_{S_\xi} G(\bar{r} \mid \bar{r}') B_j(\bar{r}') dS' dS \tag{26}$$

$$V_i = \iint_{S_\xi} T_i(\bar{r}) V(\bar{r}) dS. \tag{27}$$

To solve the new IE (11), we expand the unknown total derivatives of the charge over the **same** set of N basis functions

$$p(\bar{r}) \simeq p_N(\bar{r}) = \sum_{j=1}^{N} p_j B_j(\bar{r}'). \tag{28}$$

The charge density $q_N(\bar{r})$ given by (24) is an approximation of the exact charge distribution. The goodness of this approximation is determined by the choice of basis and test functions [13]. We use this approximate charge density to construct the right-hand side of (11). The expansion (24) is introduced in the IE (11) and the same set of test functions $T_i(\bar{r})$ is used to test (11) which leads to the equations

$$W_i - \sum_{j=1}^{N} L_{ij} q_j = \sum_{j=1}^{N} K_{ij} p_j \tag{29}$$

where

$$L_{ij} = \iint_{S_\xi} T_i(\bar{r}) \iint_{S_\xi} \bar{\nabla}' \cdot [(\bar{v}' - \bar{v}) G(\bar{r} \mid \bar{r}')] B_j(\bar{r}') dS' dS \tag{30}$$

$$W_i = \iint_{S_\xi} T_i(\bar{r}) \left[\frac{\partial}{\partial \xi} V(\bar{r}) + \bar{v} \cdot \bar{\nabla} V(\bar{r}) \right] dS' dS. \tag{31}$$

The mathematical requirements for the basis (expansion) and test (weighting) functions, used in this procedure, can be found from [13] and [14]: the basis functions must be in the domain of the operator A, given by

$$Ax = \iint_{S_\xi} G(\bar{r} \mid \bar{r}') x(\bar{r}') dS' \tag{32}$$

and simultaneously in the domain of the operator B, given by

$$Bx = \iint_{S_\xi} \bar{\nabla}' \cdot [(\bar{v}' - \bar{v}) G(\bar{r} \mid \bar{r}')] x(\bar{r}') dS'. \tag{33}$$

Furthermore, the basis functions have to form a complete set for the range of A and B. For simple basis functions such as pulse basis functions, the first requirement will normally be fulfilled, the second is much more difficult to prove. For the test functions, the main requirement is that they can represent the excitation: they have to be a proper representation of both the potential and the geometrical derivative of the potential [14].

By constructing the right-hand side with the approximate charge density $q_N(\bar{r}')$, a certain error is introduced. This error on the right hand is closely related to the error on the charge which arises from applying the MoM to (1). Little is known in the literature about this error. From a theoretical viewpoint, one can say intuitively if the operator B satisfies some property of boundedness, then the approximate right-hand side converges to the exact one when increasing the number of cells. Furthermore, one could argue that the charge distribution need not be known in a very accurate way to construct this right-hand side because an integration of the modified Green's function $\bar{\nabla}' \cdot [(\bar{v}' - \bar{v}) G(\bar{r} \mid \bar{r}')]$ with the charge distribution is performed (in most cases, this is a convolution). Numerical experiments must indicate in how far errors are introduced by this step. From the results in the examples in Sections VI, VII, and VIII we can certainly conclude that this error is negligible.

By using a single set of basis functions and a single set of test functions for both IE's, the same system matrix $\mathbf{K} = [K_{ij}]$ appears in the system of (29) as in the original system (25). Once (25) is solved and the left-hand side of (29) constructed, only N^2 arithmetic operations are needed to obtain a geometrical derivative, provided a LU-decomposition scheme is used when solving the matrix equations.

Usually, a designer is not interested in a very accurate solution for the charge density at each point but in some global observable quantities such as the total charge or the capacitance of the conductors. The total charge on the conducting surface S_ξ is given by

$$Q = \iint_{S_\xi} q(\bar{r}) dS \tag{34}$$

and the derivative with respect to the geometrical parameter ξ by

$$\frac{dQ}{d\xi} = \iint_{S_\xi} p(\bar{r}) dS + \iint_{S_\xi} q(\bar{r}) (\bar{\nabla} \cdot \bar{v}) dS \tag{35}$$

which can be evaluated once the solution for $p(\bar{r})$ and $q(\bar{r})$ is known.

The computational efficiency of the method can be appreciated by considering two possible methods for calculating derivatives. If we suppose that the surface is divided into N cells and that the structure is modified by M geometrical parameters, the total number of arithmetic operations for solving for the geometrical derivatives with the procedure described above is proportional to $N^3/3 + (M+1)N^2$. The $N^3/3$ term originates from a LU decomposition scheme. We contrast this with a central finite difference calculation of the derivative, i.e., the derivative is estimated by perturbing the planar surface twice, solving the charge density twice and taking the difference of the calculated charges or capacitances. The total number of operations in that case would be $N^3/3 + N^2 + 2M\alpha(N)N^3/3 + N^2$ where $\alpha(N)$ is a factor between zero and one (but in general closer to one) which takes into account that for inversion of the perturbed system of equations some part of the original inverse matrix can be exploited. Our method is superior in number of operations to the difference scheme by about a factor of $1 + 2M\alpha(N)$. Furthermore, we will show that the central finite difference estimate depends

crucially on the meshing of S_ξ, which is not the case for our new method.

In the next sections, the approach is illustrated by some simple electrostatic examples, where a geometrical parameter is varied over some interval. We emphasise the ideas involved and not the perfection of using the MoM. We discuss the relation between the meshing strategies by which discretization of the structure is performed in the MoM and a central difference estimate of the desired derivative, contrasting this with the geometrical derivative calculated by our new method.

VI. Capacitance of a Single Rectangular Plate

We consider the case of the capacitance of a rectangular perfectly conducting plate with width w in the x-direction and length L in the y-direction at a potential of 1 V in free space. No exact analytical solution of the charge distribution in terms of the geometrical parameters w, L and space coordinates x and y is known for this case. We vary the length L of the plate. In order to obtain the charge density, we subdivide the plate in a mesh of rectangular cells. The charge distribution and the geometrical derivative of the charge are expanded in pulse basis functions and point-matching is used for testing. The derivation of the matrix elements L_{ij}, given by (30), is straightforward and is given in the Appendix.

Two meshing strategies are followed during the expansion of the surface. For the first meshing strategy the elementary cell dimension is proportionally adapted with the length L of the plate while the total number of cells remains constant. We call this meshing strategy the "moving mesh strategy," stressing the fact that the mesh moves with the structure. In the second meshing strategy, we restrict the cell dimension to a maximum value. The total number of cells will vary with the value of L. This meshing strategy is called the "fixed mesh strategy," emphasizing the fact that the location of the cells remains fixed. We are interested in the total capacitance of the plate $C = Q_{\text{tot}}/V$, the derivative of the total capacitance of the plate with respect to the parameter L, and finally a central finite difference estimate of this derivative according to the fixed step two-point formula

$$\frac{dC}{dL} = \frac{C\left(L+\frac{h}{2}\right) - C\left(L-\frac{h}{2}\right)}{h} + O(h^2) \qquad (36)$$

where h is a small variation of the length. Capacitance values are normalized with a factor $4\pi\epsilon_0\epsilon_r$. The geometrical derivative of the capacitance, as a solution of the integral equation, is designated by IED (integral equation derivative) while the geometrical derivative, obtained with the finite difference estimate (e.g., (36)) is designated by FDD (finite difference derivative).

A. Moving Mesh Strategy

The rectangular plate of dimension 1.0 by 1.0 (in arbitrary units) is subdivided with eight divisions in the x-direction and 80 in the y-direction. We increase the length L from 1.0 to 10.0 in steps of 0.1 in the y-direction such that the dimension of a cell varies from 0.0125 to 0.125 and the total number of cells remains constant at 640 cells. We also calculated the same

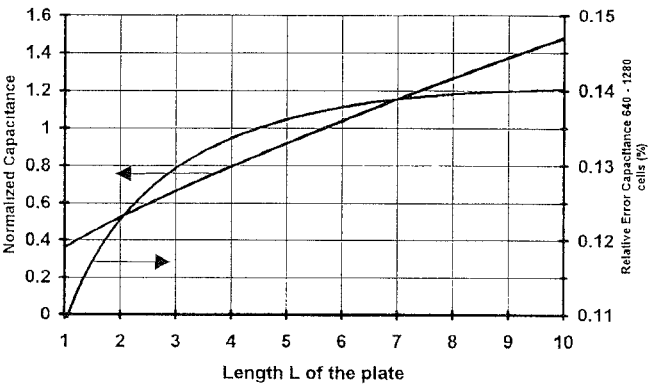

Fig 1. Capacitance and relative error between the capacitance calculated with 640 cells and the capacitance calculated with 1280 cells (moving mesh)

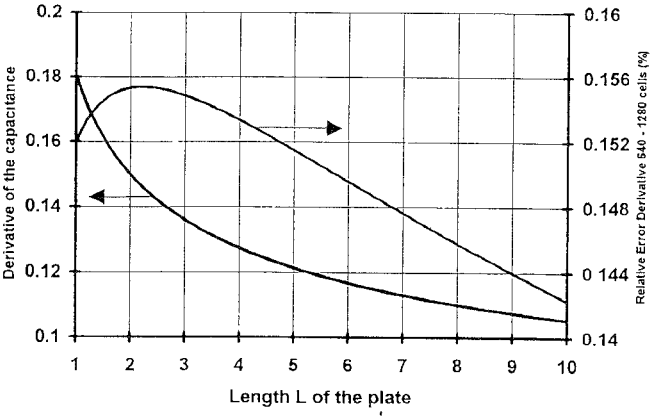

Fig. 2. Derivative of the capacitance and relative error between the derivative of the capacitance calculated with 640 cells and the derivative of the capacitance calculated with 1280 cells (moving mesh)

parameter sweep with 160 cells in the y-direction (total of 1280 cells) as a reference result. In Fig. 1 the increasing capacitance as a function of the length L is shown, together with the relative error between the capacitance calculated with 640 cells and the one, calculated with 1280 cells. As expected we see that the relative error increases with the length or, otherwise stated, the resolution of the solution (the number of basis functions per unit length) decreases with the length. In Fig. 2 the IED for the case of 640 cells and the relative error with the IED, calculated with 1280 cells is shown. The overall relative error is slightly higher than in Fig. 1 and shows a maximum. This can be understood as follows: by increasing the length with a fixed number of cells, the relative error with respect to the 1280-case for both $q(\bar{r}')$ and $\frac{\partial}{\partial\xi}q(r')+\bar{v}'\cdot\bar{\nabla}'q(\bar{r}')$ increases because resolution decreases. The total derivative of the charge however is given by a combination of the $\frac{\partial}{\partial\xi}q(\bar{r}')+\bar{v}'\cdot\bar{\nabla}'q(\bar{r}')$ and a term containing $q(\bar{r}')$ and $\bar{\nabla}\cdot\bar{v} = 1/L$ (see (35)). This last term is decreasing with the length which implies that the sum must reach a maximum for some value of L.

We now compare the IED with a two point central finite difference estimate of the capacitance for $h = 0.1$ and consider the relative error

$$E_{\text{rel}} = \frac{\left|\left(\frac{dC}{dL}\right)_{\text{IED}} - \left(\frac{dC}{dL}\right)_{\text{FDD}}\right|}{\left(\frac{dC}{dL}\right)_{\text{FDD}}}. \qquad (37)$$

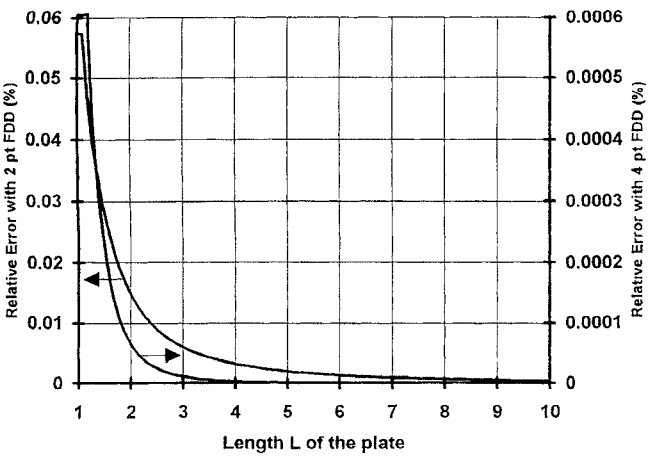

Fig. 3. Relative error between finite difference derivative (two-point and four-point) and integral equation derivative (moving mesh).

This is a measure for the correspondence between FDD $(dC/dL)_{\mathrm{FDD}}$, and the IED $(dC/dL)_{\mathrm{IED}}$. Both values $(dC/dL)_{\mathrm{FDD}}$ and $(dC/dL)_{\mathrm{IED}}$ differ from the exact value of the derivative. Large values of (37) can either be due to an incorrect calculated IED or to a poor estimate of the FDD. A poor estimate of the FDD can normally be improved by decreasing the step h or taking more points into consideration. For example, a better FDD estimate would be given by the four-point formula

$$\frac{dC}{dL} = \frac{C(L-2h) - 8C(L-h) + 8C(L+h) - C(L+2h)}{12h} + O(h^4) \tag{38}$$

The relative error for the two-point estimate (36) and the four-point estimate (38) are shown in Fig. 3. The relative errors for the four-point estimate are extremely small which leads to the conclusion that the IED almost entirely coincides with the FDD and that both values must be close to the exact value (within 0.156% of the 1280 case).

From this example, we can conclude that both the derivative of the charge and the charge itself are well represented by the chosen basis functions and that the error, introduced by approximating the right-hand side of (11), must be negligible because a FDD gives no better results than the IED. Both calculated and estimated gradients have a continuous characteristic, hence both could be used directly in an optimization procedure based on gradient information. For the central difference estimate, however, the capacitance must be evaluated twice or four times and a judicious choice of the step width of the perturbation around the central abscissa point or the number of points in the finite difference formula must be made, taking into account the rate of the variation of the capacitance. In the next subsection we will take the capacitance and the derivative of the capacitance, calculated with 1280 cells as the exact reference result.

B. Fixed Mesh Strategy

The rectangular plate with the same initial dimensions and parameter interval is meshed up in the following way: the total

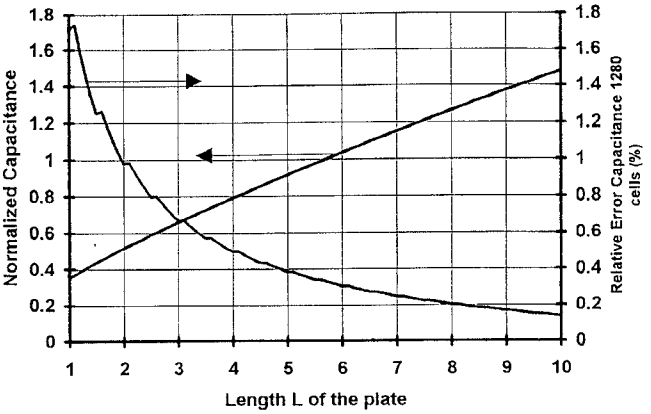

Fig. 4. Capacitance and relative error between the capacitance (fixed mesh) and the capacitance calculated with 1280 cells.

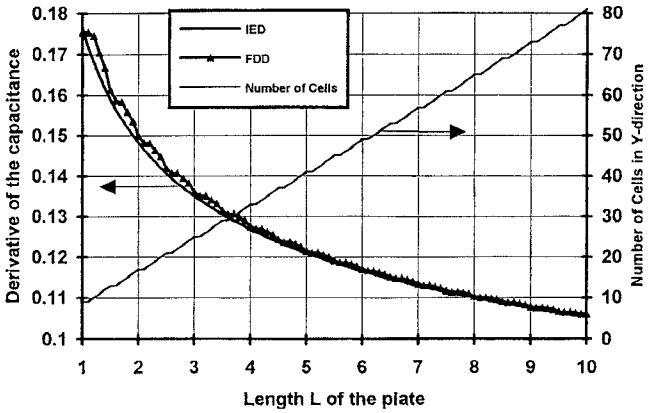

Fig. 5. Integral equation derivative of the capacitance and finite difference derivative together with the number of cells in y-direction (fixed mesh).

number of divisions varies in such a way that the inequality

$$\Delta L = \frac{L}{N_L} < \tau \tag{39}$$

is always fullfilled. Here N_L is the number of divisions in the y-direction of L and τ is the maximum dimension of one division in the y-direction. In this case the maximum is chosen to be 0.125. In Fig. 4 the capacitance and the relative error between this result and the reference result with 1280 cells is shown. As expected, this relative error is higher because of the smaller number of cells for small L values. The error decreases down to 0.14% where resolution is the same as in Fig. 1 (640 cells). Remark that the curve of the relative error is not continuous because N_L can differ for each value of L.

We first compare the IED with the FDD: Fig. 5 shows the IED and FDD in conjunction with the number of cells in the y-direction. Remark the difference between the IED-curve and the FDD-curve. The number of cells in the y-direction is steadily increasing from 9 to 80 but at certain values of L, where the inequality (39) is automatically fullfilled, the number of cells stays constant. At these values of L a discontinuous behavior of the FDD is observable. The IED, however, has a perfectly smooth characteristic. The jumpy behavior of the FDD is magnified when considering the relative error (37)

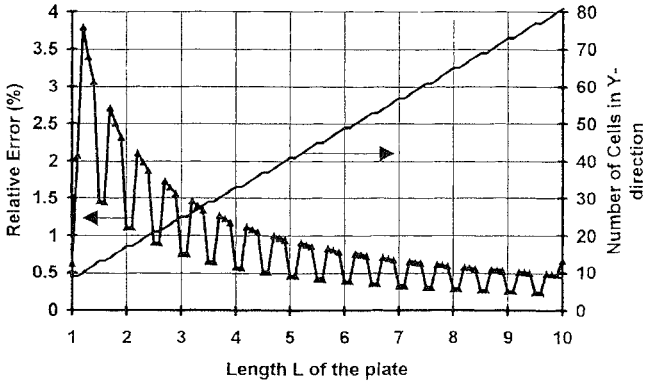

Fig. 6 Relative error between the integral equation derivative and the finite difference derivative (fixed mesh)

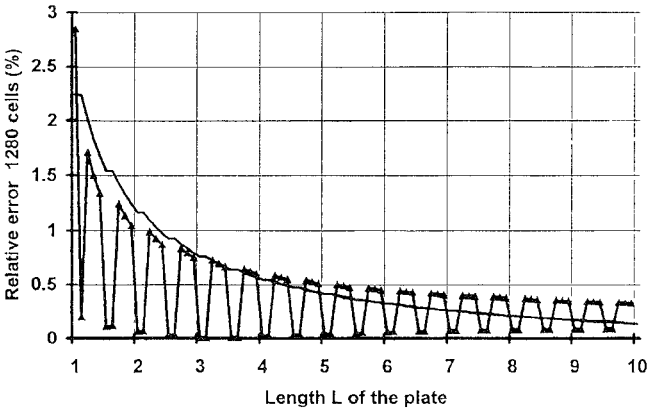

Fig 7 Relative error between the integral equation derivative and the derivative of the capacitance, calculated with 1280 cells, and relative error between the finite difference derivative and the derivative of the capacitance, calculated with 1280 cells

between the IED and the FDD (see Fig. 6). The relative error curve jumps from one higher curve to another curve when the number of cells remains constant. The relative error is small when the number of cells stays constant. However, when the number of cells changes in going from one value of L to the next one, the discretization error changes and the FDD differs more from the IED. This means that if we want to use a finite difference formula for obtaining smooth, continuous derivative estimates the same grid must be used for all parameter values and consequently the number of cells must be high enough from the beginning even for small L-values.

A comparison with the capacitance, calculated with 1280 cells, is depicted in Fig. 7. Both estimates differ from the exact reference result. The FDD is certainly not more accurate, taking into account the relative error on the capacitance itself (Fig. 4). Cancellation of discretization errors brings this estimate closer to the exact curve for small values of L but at larger values of L, the curve diverges. The FDD converges smoothly to the exact solution when resolution is increased.

The main conclusion we draw from this example is that if we change the number of cells when perturbing around some value of L, a poor discontinuous estimate will result. For a simple rectangle, as in our case, one can still choose a meshing strategy such that one knows beforehand for what values of

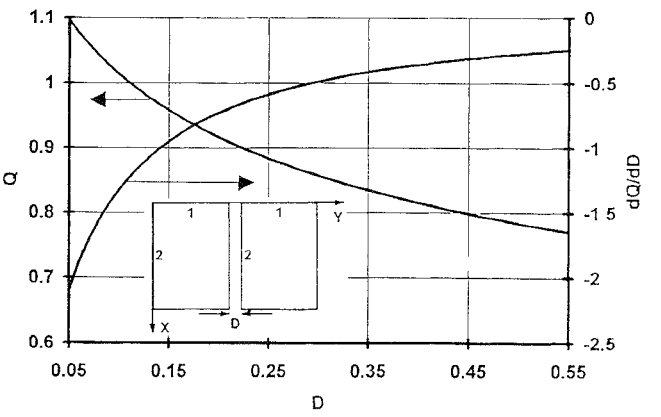

Fig. 8. Total charge and integral equation derivative of the charge

L a change in the number of divisions will occur. For a general shape however, where a mixed mesh of rectangles and triangles is used, this prediction of a change in the number of cells is much more difficult. Due to the possible discontinuous behavior, the FDD is in general not suitable for use in an optimization procedure, while the IE method proposed here does not suffer from this inconvenience.

VII. Capacitance Between Two Equiplanar Rectangular Patches as a Function of Separation Distance

The IE not only allows us to calculate the sensitivity of the charge with respect to geometrical parameters which directly modify the shape of the surfaces, such as width or length, but also with respect to geometrical parameters between surfaces. To illustrate this, we consider the case of two conducting plates in the same plane (inset of Fig. 8). The dimensions are shown on the figure. The distance D between the plates varies from 0.05 to 0.55 in steps of 0.01. The number of cells in the x-direction is 20 and 10 in the y-direction. Plate 1 is placed at 1 V and plate 2 at -1 V. In Fig. 8 the positive charge on plate 1 and the derivative of this charge with respect to the distance D is shown. The relative error between the FDD and the IED is depicted in Fig. 9. The relative error is considered for a two-point FDD (36) and a four-point FDD (38). The four-point estimate decreases the relative error over two decades which means that the FDD and IED coincide entirely. The relative error is higher at the beginning of the parameter interval because the step size 0.01 is there one-fifth of the total abscissa value.

VIII. Multilayer Multiconductor Thin Microstrip Lines

Under quasi-TEM assumptions, a general two-dimensional configuration of N microstrip lines, embedded in a multilayered medium above a ground plane, supports N eigenmodes, each characterized by their own mode-impedance and mode-velocity. For two-layered, single line microstrips, accurate analytical design formulas exist which for a given characteristic impedance gives the microstrip width to substrate height ratio [15]. For coupled lines on a one layered substrate, design

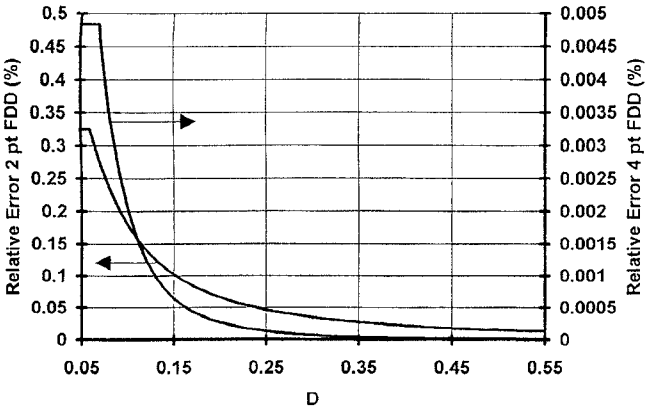

Fig. 9. Relative error between finite difference estimate (two point and four point estimate) and integral equation derivative.

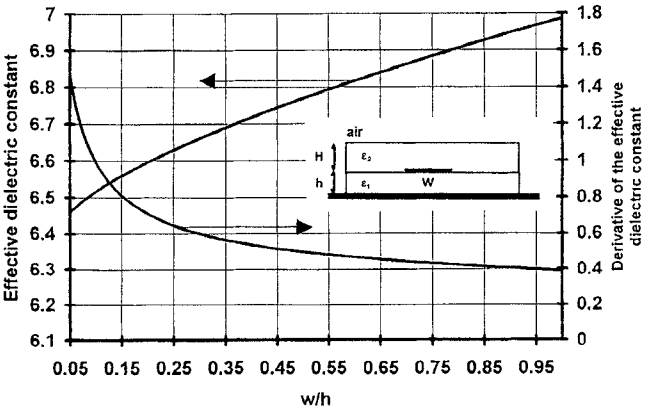

Fig. 10. Effective dielectric constant and derivative of the effective dielectric constant with respect to w/h.

formulas exist for the odd-mode impedance and even-mode impedance in terms of physical geometry [16]. For a general multiconductor transmission line more approximations—if possible—must be made to obtain analytical formulas for the geometrical dimensions in terms of mode-impedances or capacitance matrix and inductance matrix elements.

For a more accurate calculation of two-dimensional (2–D) or three-dimensional (3-D) capacitance matrices of general multiconductor interconnects in a multilayered medium the integral equation method is a commonly used technique. The integral (11) is also applicable to calculation of derivatives of capacitances of such strips. Here we will only consider infinitely thin perfectly conducting strips. In that case the surface becomes a line and the velocity $\bar{v}$ also becomes one dimensional. As the inductance calculation reduces to an equivalent so-called vacuum capacitance calculation [9], we can not only obtain geometrical derivatives of capacitances but it also becomes possible to obtain derivatives for the mode-impedances and mode-velocities and to design the physical geometry for, e.g., given mode-impedances. To illustrate this we consider two examples:

A. A Three-Layered Single Microstrip Line

As a first example we consider a microstrip in a three-layered medium [17], [18], which is depicted in Fig. 10 and where $H = 0.206h$, $\epsilon_1 = 9.6\epsilon_0$, $\epsilon_2 = 2.6\epsilon_0$ and the top layer is air. We calculate the derivative of the characteristic impedance and effective permittivity with respect to the width w of the microstrip (or w/h holding h constant). The Green's function for the layered substrate was approximated with complex images [19], [20]. The error introduced by this approximation is neglible (0.000 175% on the Green's function in the spectral domain). For the microstrip 500 pulse basis functions were used. In Fig. 10, the effective dielectric constant is shown together with the derivative with respect to the aspect ratio w/h for narrow lines ($w/h \leq 1$). In Fig. 11 the characteristic impedance and the derivative of the characteristic impedance with respect to w/h is depicted. The maximum relative error between the IED and FDD for the effective dielectric constant is 0.001 62%. The maximum relative error between the IED and the FDD for the characteristic impedance was 0.0039%.

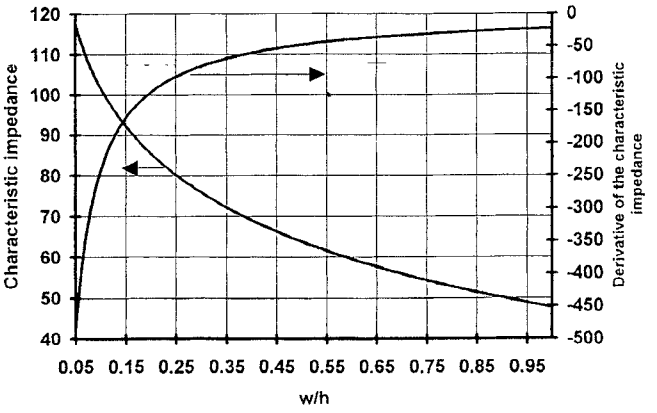

Fig. 11. Characteristic impedance and derivative of the characteristic impedance with respect to w/h.

B. Three Symmetrical Coupled Microstrip Lines

As a second example we consider a symmetrical three-line microstrip configuration as in [21]. The geometry is depicted in Fig. 12 and the dimensions are $w = h = 25$ mil, $\epsilon_r = 9.8$ and the top layer is air. These three parallel coupled lines can be used for the design of compact band-pass filters [22]. Under quasi-TEM assumption, the structure supports three fundamental modes which we denote by EE, OE, and OO as in [21]. The mode-impedances are given by

$$Z_x = \frac{1}{c\sqrt{C_{x,\text{air}}C_{x,\text{diel}}}} \tag{40}$$

where c is the velocity of light, $C_{x,\text{diel}}$ the mode capacitance, when the substrate is present, $C_{x,\text{air}}$ the mode capacitance when the substrate is replaced by air and x is equal to EE, OE or OO. These mode capacitances $C_{x,\text{diel}}$ (or $C_{x,\text{air}}$) are given in terms of the capacitance matrix elements C_{ij} as (omitting the subscript air or diel)

$$\begin{aligned}
\mu &= \frac{-(C_{11} - C_{22} + C_{13}) - \sqrt{(C_{11} - C_{22} + C_{13})^2 + 8C_{12}^2}}{2C_{12}} \\
C_{\text{OE}} &= C_{11} - C_{13} \\
C_{\text{EE}} &= C_{11} + \mu C_{12} + C_{13} \\
C_{\text{OO}} &= C_{22} - \mu C_{12}.
\end{aligned} \tag{41}$$

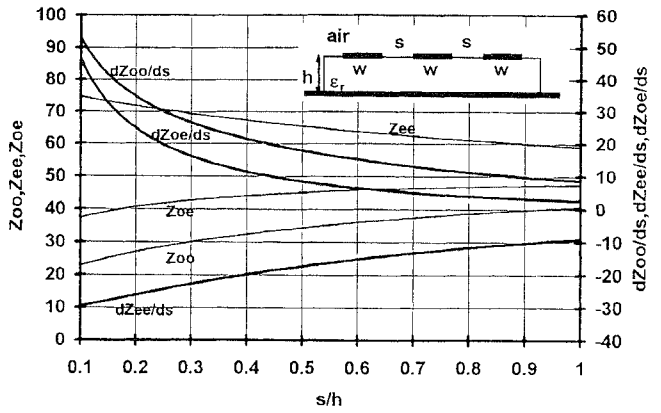

Fig 12. Impedance of the EE-, OE- and OO-mode and derivatives with respect to s as a function of s/h for $w/h = 1$.

Once the capacitance matrix and the derivative of the capacitance matrix with respect to a geometrical parameter have been determined, the derivatives of the mode-impedances can easily be found. For each strip 100 basis functions were used. The mode-impedances together with the derivatives with respect to the parameter s (or s/h, holding h constant) are calculated with the method presented above and shown in Fig. 12. Again excellent agreement with a FDD was obtained.

IX. Conclusion

A new IE for the derivative of the charge with respect to some geometrical parameter has been derived using a transport theorem. The geometrical parameter modifies the shape of the surface or is related to distances between the surfaces. The solution of the new IE can be efficiently found by solving for the charge density by the MoM, substituting the charge solution in the new IE and applying the MoM on the new IE with the same set of basis functions and test functions as used for solving the original IE. We showed the applicability of this procedure for various planar three dimensional and two dimensional capacitance calculations. The obtained derivatives are perfectly continuous and smooth and above all this continuity is independent of the structure meshing, contrary to derivatives which are obtained by a central finite difference estimate. Most of all we emphasise the fact that no perturbed geometry problem must be solved, since the derivatives are obtained from one single solution of the problem. Thus, a computationally efficient method, based on an accurate integral equation technique, has been developed to obtain the sensitivity of the solution with respect to a geometrical parameter. Futhermore, it was shown that our method can also be used to obtain derivatives for mode impedances and mode velocities as illustrated for some coupled microstrip line configurations.

Appendix

A. Potential Due to a Uniformly Charged Rectangle

Consider a uniformly charged rectangle with dimensions Δx_j and Δy_j and center point (x_j, y_j, z_j). The potential per unit charge $V(x, y, z)$ is given by [8]

$$V(x,y,z) = \frac{1}{4\pi\epsilon_0\epsilon_r}\int_{x_1}^{x_2}\int_{y_1}^{y_2} \times \frac{1}{((y'-y)^2+(x'-x)^2+Z^2)^{1/2}}dx'dy' \quad (42)$$

where $Z = z - z_j$ remains constant and where

$$x_1 = x_j - \frac{\Delta x_j}{2} \quad x_2 = x_j + \frac{\Delta x_j}{2}$$
$$y_1 = y_j - \frac{\Delta y_j}{2} \quad y_2 = y_j + \frac{\Delta y_j}{2} \quad (43)$$

After integration (42) yields

$$\begin{aligned} V(x,y,z) = \frac{1}{4\pi\epsilon_0\epsilon_r}\Bigg\{ & (x_j - x)\log\left[\frac{(c+A)(d+B)}{(d+C)(c+D)}\right] \\ & + \frac{\Delta x_j}{2}\log\left[\frac{(d+B)(d+C)}{(c+D)(c+A)}\right] \\ & + (y_j - y)\log\left[\frac{(a+A)(b+B)}{(b+D)(a+C)}\right] \\ & + \frac{\Delta y_j}{2}\log\left[\frac{(b+B)(b+D)}{(a+C)(a+A)}\right] \\ & - Z\arctan\left[\frac{ac}{ZA}\right] - Z\arctan\left[\frac{bd}{ZB}\right] \\ & + Z\arctan\left[\frac{ad}{ZC}\right] + Z\arctan\left[\frac{bc}{ZD}\right]\Bigg\} \end{aligned} \quad (44)$$

where

$$a = x_j - \frac{\Delta x_j}{2} - x \quad b = x_j + \frac{\Delta x_j}{2} - x$$
$$c = y_j - \frac{\Delta y_j}{2} - y \quad d = y_j + \frac{\Delta y_j}{2} - y \quad (45)$$
$$A = \sqrt{a^2+c^2+Z^2} \quad B = \sqrt{b^2+d^2+Z^2}$$
$$C = \sqrt{a^2+d^2+Z^2} \quad D = \sqrt{b^2+c^2+Z^2}. \quad (46)$$

B. Calculation of the Matrix Elements L_{ij}

In the case the velocity vector is given by $\bar{v} = \alpha y \bar{u}_y$, the matrix elements L_{ij} in free space can be written as follows

$$L_{ij} = \frac{\alpha}{4\pi\epsilon_0\epsilon_r}\int_{x_2}^{x_1}\int_{y_2}^{y_1}\frac{\partial}{\partial y'} \times \left\{\frac{(y'-y_i)}{((x'-x_i)^2+(y'-y_i)^2+Z^2)^{1/2}}\right\}dx'dy' \quad (47)$$

where (x_i, y_i, z_i) is the center point of the observation cell. This can be simplified into the following result

$$L_{ij} = \frac{\alpha}{4\pi\epsilon_0\epsilon_r}\left\{d\log\left[\frac{b+B}{a+C}\right] - c\log\left[\frac{b+D}{a+A}\right]\right\} \quad (48)$$

with the same notations as in (45) and (46) but with the x replaced by x_i and the y by y_i.

Acknowledgment

The authors would like to thank the reviewers for their valuable suggestions.

REFERENCES

[1] J. Sabonnadiere and A. Konrad, "Computing em fields," *IEEE Spectrum*, pp. 52–56, Nov. 1992.

[2] J. W. Bandler, "Minimax microstrip filter design using direct EM field simulation," in *IEEE Microwave Theory Techniques Soc. Int. Symp. Dig.*, 1993, pp. 889–892.

[3] L. Ji-Fuh and A. Z. Kawthar, "CAD of microwave junctions by polynomial curve fitting," in *IEEE Microwave Theory Tech. Soc. Int. Symp. Dig.*, 1993, pp. 451–454.

[4] S. Ratnajeevan and H. Hoole, "Artificial neural networks in the solution of inverse electromagnetic field problems," *IEEE Trans. Magn.*, vol. 29, no. 2, pp. 1931–1934, Mar. 1993.

[5] P. Garcia and J. P. Webb, "Optimization of planar devices by the finite element method," *IEEE Trans. Microwave Theory Tech.*, vol. 38, no. 1, pp. 48–53, Jan. 1990.

[6] A. Farrar and A. T. Adams, "Matrix methods for microstrip three-dimensional problems," *IEEE Trans. Microwave Theory Tech.*, vol. 20, no. 8, pp. 497–503, Aug. 1976.

[7] P. Benedek and P. Silvester, "Capacitance of parallel rectangular plates separated by a dielectric sheet," *IEEE Trans. Microwave Theory Tech.*, vol. 20, no. 8, pp. 504–510, Aug. 1976.

[8] S. Ratnajeevan and H. Hoole, *Computer-Aided Analysis and Design of Electromagnetic Devices*. New York: Elsevier, 1989.

[9] N. Faché, F. Olyslager, and D. De Zutter, "Electromagnetic and circuit modeling of multiconductor transmission lines," *The Oxford Engineering Science Series-35*. Oxford: Clarendon Press, 1993.

[10] T. Chen-To, *Generalized Vector and Dyadic Analysis*. Piscataway, NJ: IEEE Press, 1992.

[11] J. V. Bladel, "Singular electromagnetic fields and sources," *The Oxford Engineering Science Series-28*. Oxford: Clarendon Press, 1991.

[12] S. Coen and G. M. Gladwell, "A legendre approximation method for the circular microstrip disk problem," *IEEE Trans. Microwave Theory Tech.*, vol. 25, no. 1, pp. 1–6, Jan. 1975.

[13] T. K. Sarkar, A. R. Djordjevic, and E. Arvas, "On the choice of expansion and weighting functions in the numerical solution of operator equations," *IEEE Trans. Antennas Propagat.*, vol. 33, no. 9, pp. 988–996, Sept. 1985.

[14] T. K. Sarkar, "A note on the choice of weighting functions in the method of moments," *IEEE Trans. Antennas Propagat.*, vol. 33, no. 4, pp. 436–441, Apr. 1985.

[15] H. A. Wheeler, "Transmission-line properties of parallel strips separated by a dielectric sheet," *IEEE Trans. Microwave Theory Tech.*, vol. 13, no. 3, pp. 172–185, Mar. 1965.

[16] A. Sina, R. R. Thomas, and P. B. Johns, "The design of coupled microstrip lines," *IEEE Trans. Microwave Theory Tech.*, vol. 23, no. 6, pp. 486–492, June 1975.

[17] A. Farrar and A. T. Adams, "Multilayer microstrip transmission lines," *IEEE Trans. Microwave Theory Tech.*, vol. 22, no. 10, pp. 889–891, Oct. 1974.

[18] J. Svacina, "Analysis of multilayer microstrip lines by a conformal mapping method," *IEEE Trans. Microwave Theory Tech.*, vol. 40, no. 4, pp. 769–772, Apr. 1992.

[19] Y. L. Chow, J. J. Yang, and G. E. Howard, "Complex images for electrostatic field computation in multilayered media," *IEEE Trans. Microwave Theory Tech.*, vol. 39, no. 7, pp. 1120–1125, July 1991.

[20] K. S. Oh, D. Kuznetsov, and J. E. Shutt-Aine, "Capacitance computations in a multilayered dielectric medium using closed form spatial green's functions," *IEEE Trans. Microwave Theory Tech.*, vol. 42, no. 8, pp. 1443–1453, Aug. 1994.

[21] D. Pavlidis and H. L. Hartnagel, "The design and performance of three line microstrip couplers," *IEEE Trans. Microwave Theory Tech.*, vol. 24, no. 10, pp. 631–640, Oct. 1976.

[22] R. Schwindt and C. Nguyen, "A new compact bandpass filter employing three parallel coupled lines," in *IEEE Microwave Theory Tech. Soc. Int. Symp. Dig.*, 1994, pp. 245–246.

Jan Ureel (S'91) was born in Veurne, Belgium, on July 18, 1969. He received a degree in electrical engineering from the University of Gent, Belgium, in July 1992. He is currently working toward the Ph.D. degree at the Department of Information Technology in Gent.

His current research interests are optimization theory and techniques and the simulation of planar microwave structures.

Daniël De Zutter (M'92) was born in Eeklo, Belgium, on November 8, 1953. He received a degree in electrical engineering from the University of Gent, Belgium, in July 1976. In October 1981, he obtained a Ph.D. degree and in the spring of 1984 he completed a thesis leading to a degree equivalent to the French Aggrégation or the German Habilitation.

From 1976 to 1984 he was a Research and Teaching Assistant in the Laboratory of Electromagnetism and Acoustics (now the Department of Information Technology) at the University of Gent, Belgium. He is now a Professor at the Department of Information Technology, University of Gent, and Research Director of the National Science Foundation of Belgium. Most of his earlier scientific work dealt with the electrodynamics of moving media, with emphasis on the Doppler effect and on Lorentz forces. His research now focuses on all aspects of circuit and electromagnetic modeling of high-speed and high-frequency interconnections, on electromagnetic compatibility (EMC) and electromagnetic interference (EMI) topics and on indoor propagation. As author or co-author he has contributed to 60 international journal papers and 70 papers in conference proceedings.

Dr. De Zutter received the 1995 Microwave Prize Award.